Contribution from the Departments of Chemistry, University of California, Santa Barbara, California 93106, and University of Chicago, Chicago, Illinois 60601

# Electronic Effects of Substitution Chemistry in the $KTiOPO_4$ Structure Field: Structure and Optical Properties of Potassium Vanadyl Phosphate

Mark L. F. Phillips,† William T. A. Harrison,† Thurman E. Gier,† Galen D. Stucky,*,† Gururaj V. Kulkarni,‡ and Jeremy K. Burdett‡

*Received October 25, 1989*

Potassium titanyl phosphate (KTP) is a remarkable nonlinear optic/electrooptic material whose crystal structure permits the facile substitution of many isovalent ions for K, Ti, and P. Subtle structural and electronic influences result, sometimes causing dramatic changes in NLO properties. Replacing Ti with V yields potassium vanadyl phosphate (KVP), which is structurally very similar to KTP but nearly opaque in the visible region due to the decreased energy of the vanadium $d\pi$ charge-transfer band. $KVOPO_4$ is orthorhombic, space group $Pna2_1$, with $a$ = 12.816 (5) Å, $b$ = 6.388 (2) Å, and $c$ = 10.556 (5) Å. There are two $KVOPO_4$ units per asymmetric unit, and $Z$ = 8. Optical absorption at 532 nm inhibits SHG intensity in KVP if 1.064-$\mu$m radiation is used as the pump source. The anionic group model was extended to predict the contribution to $\beta_{ijk}$ from the d electron in KVP, and it is concluded that $t_{2g}$ occupancy should not affect optical nonlinearity. The electronic influence of the $K^+$ ion on the mixing coefficient of valence and charge-transfer bands is less significant in KTP and KVP than is the analogous cation-framework interaction in $AgTiOPO_4$ and $\beta$-$NaTiOPO_4$, in which this influence results in a diminished NLO response.

## 1. Introduction

The interest in materials isostructural to the compound $KTiOPO_4$ (KTP) originates in this material's success as a nonlinear optical medium. Since its debut as a crystal for second harmonic generation (SHG) in 1976,[1] KTP has become the material of choice for the type II doubling of Nd:YAG laser light at 1.064 $\mu$m. Its desirability is due to its high power conversion efficiency and high damage threshold,[2] its extremely low onset power threshold,[3] and the low temperature sensitivity of its phase matching angle and low walkoff angle at this wavelength,[1] in addition to its physical stability and chemical inertness.[4] KTP also holds great promise for other NLO applications such as sum-and-difference frequency mixing,[5] optical parametric oscillation (OPO),[6] and electrooptic modulation,[7] where KTP-based channel waveguides may compete with Ti:$LiNbO_3$ waveguide modulators for device applications.

Like all crystalline materials with nonzero second-order nonlinear coefficients, KTP is noncentrosymmetric. The X-ray crystal structure of KTP was solved by Tordjman et al.,[8] who found that there are two crystallographically distinct sites for each of the cations and ten independent oxygen atom positions in the orthorhombic (space group $Pna2_1$) unit cell. The structure of KTP consists of infinite chains of vertex-sharing $TiO_6$ octahedra cross-linked by phosphate groups to create a 3-dimensional network. The 8- and 9-coordinate potassium atoms occupy 1-dimensional channels parallel to [001], which can be completely replaced by or exchanged with other small monovalent cations such as $Na^+$,[9] $Ag^+$,[10] $Tl^+$,[11] $NH_4^+$,[12] and $Rb^+$.[11]

In all SHG-active Ti-containing KTP isostructures characterized to date the Ti coordination environment contains a short (<1.75 Å) "titanyl" bond trans to a long (>2.10 Å) Ti-O bond. The Ti-O coordination sphere can thus be viewed as a distorted octahedral field in which the Ti is displaced from the center of the octahedron by approximately 0.15 Å. Other metal oxide NLO materials such as perovskites and tungsten bronzes exhibit similar distortions from perfect octahedral symmetry. This structural feature is the focus of several models seeking to define a structure/property paradigm for second-order nonlinear optic materials. In one of these models, the bond alternation found in perovskites, linear chain compounds, and several cyclic systems is understood in terms of a "second-order Jahn-Teller effect" that couples the (largely oxygen) nonbonding levels at the top of the oxygen p band with the metal-oxygen antibonding levels of the metal d band.[13] In this paper this idea is extended to the KTP structure type, particularly the isostructural phase $KVOPO_4$. This $d^1$ transition-metal atom gives us the opportunity to examine the effect of $t_{2g}$ electron occupancy on the KTP structure and how it influences the electronic states. Additionally, the orbital mixing described above is used to explain the existence of the strong second-order nonlinearity seen in several members of the KTP structure field and the lack of significant NLO effects in others.

## 2. Experimental Section

Crystals of $KVOPO_4$ were grown by the hydrothermal method. A 0.083-g amount of $V_2O_4$ (Alfa), 0.544 g of $KH_2PO_4$ (Fisher), 0.228 g of $K_2HPO_4 \cdot 3H_2O$ (Fisher), and 0.50 mL of deionized water were sealed in a collapsible gold tube of 0.25-in. diameter and approximately 2.5-in. length. The tube was placed in a Leco Tem-Pres bomb, which was filled with water, pressurized to 2.4 kbar, and heated to 700 °C. This temperature was maintained for 10 h, after which the bomb was cooled to 500 °C at a constant rate over 80 h. The bomb was then allowed to cool to room temperature. The product, consisting of powder and irregularly shaped crystals, was recovered by filtration, washed with water, and air-dried. A 0.175-g amount of pure dark orange crystals of $KVOPO_4$ was recovered.

KVP powder was also prepared by combining 0.415 g of $V_2O_4$, 2.45 g of $KH_2PO_4$, 2.74 g of $K_2HPO_4 \cdot 3H_2O$, and 5.0 mL of degassed $H_2O$ in a Teflon vessel. The contents were $N_2$-sparged, sealed, and shaken vigorously. The vessel was autoclaved at 200 °C under autogenous pressure for 5 days and then cooled. The product, a dark brown powder, was recovered by filtration, washed with water, and air-dried.

The $KTi_{1-x}V_xOPO_4$ (KTVP) compositions were prepared by treating mixtures of $TiCl_4$ and $V_2O_4$ in the appropriate mole ratio with $K_2HPO_4 \cdot 3H_2O$ and water, adding $KH_2PO_4$ as necessary to maintain the pH of the solution near 7. The route by which $KTi_{0.95}V_{0.05}OPO_4$ was prepared is typical of this synthetic scheme: 0.021 g of $V_2O_4$ and 3.23 g of a 1.82 M aqueous solution of $TiCl_4$ were combined with 6.85 g of $K_2HPO_4 \cdot 3H_2O$ and 5.0 mL of degassed $H_2O$ in a Teflon vessel. After the resulting hydrogel was sparged with $N_2$, the vessel was sealed and then

* To whom correspondence should be addressed.
† University of California.
‡ University of Chicago.

(1) Zumsteg, F. C.; Bierlein, J. D.; Gier, T. E. *J. Appl. Phys.* **1976**, *47*, 4980.
(2) Fan, T. Y.; Huang, C. E.; Hu, B. Q.; Eckhardt, R. C.; Fan, Y. X.; Byer, R. L.; Feigelson, R. S. *Appl. Opt.* **1987**, *26*, 2391.
(3) Eimerl, D. *Proc. SPIE-Int. Soc. Opt. Eng.* **1986**, *681*, 5.
(4) Belt, R. F.; Gashurov, G.; Liu, Y. S. *Laser Focus* **1985**, 110.
(5) (a) Baumert, J. C.; Schellenberg, F. M.; Lenth, W.; Risk, W. P.; Bjorklund, G. C. *Appl. Phys. Lett.* **1987**, *51*, 2192. (b) Risk, W. P.; Baumert, J. C.; Bjorklund, G. C.; Schellenberg, F. M.; Lenth, W. *Appl. Phys. Lett.* **1988**, *52*, 85.
(6) Vanherzeele, H.; Bierlein, J. D.; Zumsteg, F. C. *Appl. Opt.* **1988**, *27*, 3314.
(7) Bierlein, J. D.; Ferretti, A.; Brixner, L. H.; Hsu, W. Y. *Appl. Phys. Lett.* **1987**, *50*, 1216.
(8) Tordjman, I.; Masse, R.; Guitel, J. C. *Z. Kristallogr.* **1974**, *139*, 103.
(9) Phillips, M. L. F.; Harrison, W. T. A.; Gier, T. E.; Stucky, G. D. *Proc. SPIE-Int. Soc. Opt. Eng.* **1989**, *1104*, 225.
(10) Phillips, M. L.; Gier, T. E.; Eddy, M. M.; Keder, N. L.; Stucky, G. D.; Bierlein, J. D. *Solid State Ionics* **1989**, *32/33*, 147-153.
(11) Masse, R.; Grenier, J. C. *Bull. Soc. Fr. Mineral. Cristallogr.* **1971**, *94*, 437.
(12) Eddy, M. M.; Gier, T. E.; Keder, N. L.; Stucky, G. D.; Cox, D. E.; Bierlein, J. D.; Jones, G. *Inorg. Chem.* **1988**, *27*, 1856.
(13) Burdett, J. K.; Hughbanks, T. *Inorg. Chem.* **1985**, *24*, 1741. Burdett, J. K. *Inorg. Chem.* **1985**, *24*, 2244.

0020-1669/90/1329-2158$02.50/0 

**Table I.** Crystallographic Data for $KVOPO_4$

| | |
|---|---|
| formula of asym unit: $K_2V_2P_2O_{10}$ | fw = 402.0 |
| $a$ = 12.816 (5) Å | space group $Pna2_1$ (No. 33) |
| $b$ = 6.388 (2) Å | $T$ = 22 °C |
| $c$ = 10.556 (5) Å | $\lambda$ = 0.71069 Å |
| $\alpha = \beta = \gamma$ = 90° | $\rho_{calc}$ = 3.09 g/cm$^3$ |
| $V$ = 864.2 (6) Å$^3$ | $\mu$ = 34.64 cm$^{-1}$ |
| $Z$ = 8 | $R(F_o)$ = 5.64%, $R_w(F_o)$ = 5.56% |

**Table II.** Final Atomic Positions and Thermal Parameters for Potassium Vanadyl Phosphate

| atom | $x/a$ | $y/b$ | $z/c$ | $U$(equiv), Å$^2$ |
|---|---|---|---|---|
| K(1) | 0.3819 (2) | 0.7815 (4) | 0.3173 (3) | 0.0245 |
| K(2) | 0.1032 (2) | 0.7056 (4) | 0.0701 (3) | 0.0242 |
| V(1) | 0.3761 (1) | 0.4967 (2) | 0.0003 (2) | 0.0105 |
| V(2) | 0.2486 (1) | 0.2734 (2) | 0.2520 (2) | 0.0101 |
| P(1) | 0.4978 (2) | 0.3308 (3) | 0.2614 (3) | 0.0093 |
| P(2) | 0.1805 (1) | 0.4985 (4) | 0.5155 (3) | 0.0085 |
| O(1) | 0.4835 (6) | 0.477 (1) | 0.1486 (6) | 0.0127 |
| O(2) | 0.5100 (6) | 0.473 (1) | 0.3821 (6) | 0.0153 |
| O(3) | 0.3988 (5) | 0.196 (1) | 0.2842 (7) | 0.0109 |
| O(4) | 0.5941 (5) | 0.188 (1) | 0.2451 (7) | 0.0100 |
| O(5) | 0.1113 (5) | 0.306 (1) | 0.5450 (6) | 0.0125 |
| O(6) | 0.1102 (5) | 0.688 (1) | 0.4866 (7) | 0.0105 |
| O(7) | 0.2534 (6) | 0.538 (1) | 0.6326 (6) | 0.0133 |
| O(8) | 0.2558 (6) | 0.454 (1) | 0.4049 (6) | 0.0129 |
| O(9) | 0.2726 (6) | 0.463 (1) | 0.1471 (6) | 0.0138 |
| O(10) | 0.2212 (6) | 0.032 (1) | 0.3969 (7) | 0.0150 |

autoclaved in the same fashion described for KVP powder. The products were worked up by filtration and washed with water.

A good-quality single crystal of approximate dimensions 0.3 × 0.2 × 0.1 mm was mounted on a glass fiber with "superglue" prior to data collection on an automated Huber four-circle X-ray diffractometer (graphite-monochromated Mo K$\alpha$ radiation, $\lambda$ = 0.71069 Å), interfaced to a DEC Micro VAX-II computer with Crystal Logic stepping motor controllers. The orthorhombic unit cell constants were determined from 25 centered reflections and refined by least-squares methods to final values of $a$ = 12.816 (5), $b$ = 6.388 (2), and $c$ = 10.556 (5) Å. Intensity data were collected by using the $\theta$–$2\theta$ scan method, with a scan rate of 6°/min from 1.3° below K$\alpha$1 to 1.6° above K$\alpha$2. Measurements were made out to 65° in $2\theta$, giving a total of 2420 reflections. Systematic absences indicated two possible space groups: acentric $Pna2_1$, as found for other KTP isostructures, or centric $Pnam$. Three reflections monitored every hundred observations showed no systematic trends. During data reduction, the observations were corrected for absorption on the basis of the $\psi$ scans of two reflections. After merging ($R$ = 3%), 1431 independent reflections were considered observed, on the basis of the criterion $I > 3\sigma(I)$. The KTP structure was used as a starting model in the space group $Pna2_1$, and the final anisotropic refinement on $F$ converged to give agreement values of $R$ = 5.64% and $R_w$ = 5.56% for 146 parameters. All least-squares and subsidiary calculations were performed by using the Oxford CRYSTALS system,[14] and an isotropic secondary extinction correction was included in the final cycles of refinement.[15] A list of crystallographic data for $KVOPO_4$ is presented in Table I, and final observed and calculated structure factors are available as supplementary material.

The purity of all products was ascertained by X-ray powder diffraction using a Scintag automated $\theta$–$\theta$ powder diffractometer, using Cu K$\alpha$ radiation ($\lambda$ = 1.5406 Å). The patterns were indexed on the basis of the single-crystal unit cell constants, and refined lattice parameters and esd's were obtained with Scintag routines. UV–visible spectra were recorded on the powder samples by using a Cary 14 UV–visible–IR spectrophotometer operating in diffuse-reflectance mode. Powder SHG intensity data were obtained at 1064 nm with a system similar to that described by Dougherty and Kurtz.[16] Data were collected from samples of uniform crystallite size in reflectance mode, and the intensity of the second harmonic light from the sample was measured relative to the SHG intensity at the reference channel. A Kigre MK-367 Nd:YAG laser was the source of the 1064-nm light, producing 20-mJ, 4-ns pulses in single-shot mode. Intensities were measured by using a Tektronix 2467B 400 MHz oscilloscope with a DCS01 digitizing camera system. Magnetic susceptibility data were obtained on KVP between 5 and 50 K with a liquid-helium-cooled SQUID magnetometer.

(14) Watkin, D. J.; Carruthers, J. R.; Betteridge, P. W. *CRYSTALS User Guide*; Chemical Crystallography Laboratory: Oxford, U.K., 1985.
(15) Complex, neutral-atom scattering factors were obtained from: *International Tables for X-ray Crystallography*; International Union for Crystallography: Birmingham, U.K., 1974; Vol. IV, Table 2A.
(16) Dougherty, J. P.; Kurtz, S. K. *J. Appl. Crsytallogr.* **1976**, *9*, 145–147.

**Table III.** Selected Bond Distances and Angles for $KVOPO_4$

Distances (Å)

| | | | |
|---|---|---|---|
| V(1)–O(1) | 2.089 (7) | P(2)–O(8) | 1.541 (8) |
| V(1)–O(2) | 1.930 (7) | K(1)–O(1) | 2.943 (8) |
| V(1)–O(5) | 2.040 (7) | K(1)–O(2) | 2.653 (9) |
| V(1)–O(6) | 1.986 (7) | K(1)–O(3) | 2.679 (7) |
| V(1)–O(9) | 2.051 (7) | K(1)–O(5) | 2.880 (7) |
| V(1)–O(10) | 1.673 (8) | K(1)–O(7) | 3.081 (8) |
| V(2)–O(3) | 2.016 (7) | K(1)–O(8) | 2.800 (8) |
| V(2)–O(4) | 1.997 (6) | K(1)–O(9) | 3.053 (8) |
| V(2)–O(7) | 1.962 (7) | K(1)–O(10) | 2.741 (8) |
| V(2)–O(8) | 1.987 (7) | K(2)–O(1) | 2.675 (8) |
| V(2)–O(9) | 1.671 (8) | K(2)–O(2) | 2.995 (9) |
| V(2)–O(10) | 2.199 (8) | K(2)–O(3) | 3.019 (8) |
| P(1)–O(1) | 1.524 (8) | K(2)–O(4) | 3.123 (7) |
| P(1)–O(2) | 1.574 (8) | K(2)–O(5) | 2.764 (7) |
| P(1)–O(3) | 1.553 (7) | K(2)–O(7) | 2.884 (8) |
| P(1)–O(4) | 1.543 (6) | K(2)–O(8) | 2.971 (8) |
| P(2)–O(5) | 1.545 (7) | K(2)–O(9) | 2.787 (8) |
| P(2)–O(6) | 1.540 (7) | K(2)–O(10) | 3.104 (8) |
| P(2)–O(7) | 1.570 (7) | | |

Angles (deg)

| | | | |
|---|---|---|---|
| V(1)–O(9)–V(2) | 134.0 (4) | V(1)–O(10)–V(2) | 131.9 (4) |
| O(10)–V(1)–O(9) | 91.4 (3) | O(10)–V(2)–O(9) | 177.2 (4) |

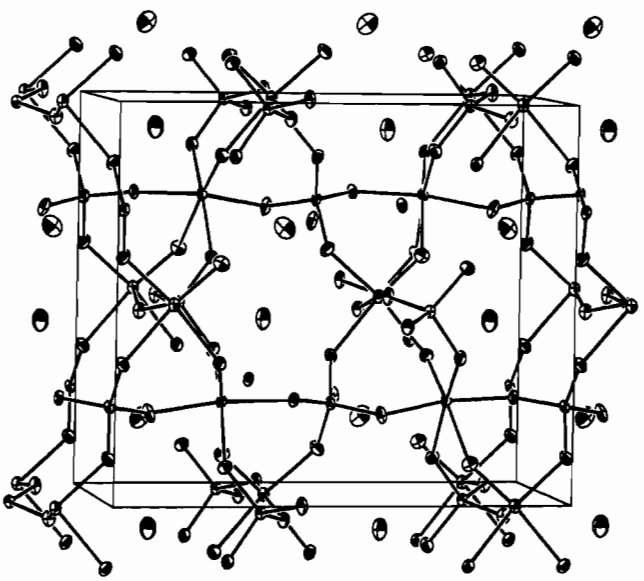

**Figure 1.** Oblique view of KVP (010) plane, showing $VO_6$ chains.

### 3.1. Structure

The final atomic positional and thermal parameters for potassium vanadyl phosphate are given in Table II. As in KTP, there are two crystallographically distinct potassium atoms (irregular 8- and 9-coordination), two vanadium atoms (distorted octahedra), and two phosphorus sites (tetrahedral). Eight of the ten distinct oxygen atoms are involved in V–O–P links, and the remaining two (O(9) and O(10)) participate in V–O–V bonds. All of the oxygen atoms except O(6) also coordinate to either or both potassium atoms. Selected final bond distance and angle data are presented in Table III.

KVP adopts the orthorhombic structure found for all KTP-type materials and, in particular, a configuration in the $VO_6$ chains very similar to that found in the $TiO_6$ chains in KTP itself (Figure 1). Around V(1), the oxygen atoms in the V–O–V chain (O(9) and O(10)) are in cis configuration; around V(2), the same two oxygens are approximately trans. The short–long bond length alteration found in KTP is present to an even greater extent in KVP, as illsutrated in Figure 2. The V(1) octahedron shows about the same degree of distortion as the Ti(1) octahedron in KTP, while the V(2) octahedron is even less regular than that of Ti(2)

**Table IV.** Average Trans Ti–O Distances ($R_{av}$) and Bond Length Differences ($\Delta_{Ti}$) in the KTP Structure Field

| compd | $R_{av}$(Ti(1)), Å | $\Delta_{Ti(1)}$, Å | $R_{av}$(Ti(2)), Å | $\Delta_{Ti(2)}$, Å | ref |
|---|---|---|---|---|---|
| $KTiOPO_4$ | 1.940 (6) | 0.443 (6) | 1.920 (6) | 0.363 (6) | 8 |
| $KVOPO_4$ | 1.88 (1) | 0.42 (1) | 1.94 (1) | 0.53 (1) | this work |
| $NH_4TiOPO_4$ | 1.932 (5) | 0.438 (5) | 1.919 (6) | 0.354 (6) | 12 |
| $TlTiOPO_4$ | 1.940 (7) | 0.429 (7) | 1.912 (7) | 0.329 (7) | 26 |
| $RbTiOPO_4$ | 1.940 (6) | 0.426 (7) | 1.922 (7) | 0.344 (7) | 27 |
| $AgTiOPO_4$ | 1.97 (2) | 0.52 (2) | 1.93 (2) | 0.29 (2) | 10 |
| $\beta$-$NaTiOPO_4$ | 1.972 (8) | 0.515 (8) | 1.929 (8) | 0.347 (8) | 9 |
| $(NH_4)_{0.5}H_{0.5}TiOPO_4$ | 1.924 (6) | 0.046 (6) | 1.939 (7) | −0.350 (7) | 12 |
| $(NH_4)_{0.5}(H_3O)_{0.5}TiOPO_4$ | 1.92 (4) | 0.45 (4) | 1.92 (3) | 0.25 (3) | 12 |
| $KTiOAsO_4$ | 1.94 (2) | 0.40 (2) | 1.93 (3) | 0.33 (3) | 28 |
| $KTiO(PO_4)_{0.5}(AsO_4)_{0.5}$ | 1.94 (1) | 0.43 (1) | 1.93 (1) | 0.33 (1) | 29 |
| $K_{0.5}(NH_4)_{0.5}TiOAsO_4$ | 1.94 (2) | 0.42 (2) | 1.94 (2) | 0.36 (2) | 9 |
| $KGaPO_4F_{0.7}(OH)_{0.3}$ | 1.928 (8) | −0.027 (8) | 1.953 (8) | 0.056 (8) | 10 |
| $TlTiOPO_4$ (650 °C) | 1.94 (1) | 0.23 (1) | 1.90 (1) | 0.00 (1) | 26 |
| $KSnOPO_4$ | 2.04 (1) | 0.14 (1) | 1.97 (1) | 0.01 (1) | 30 |

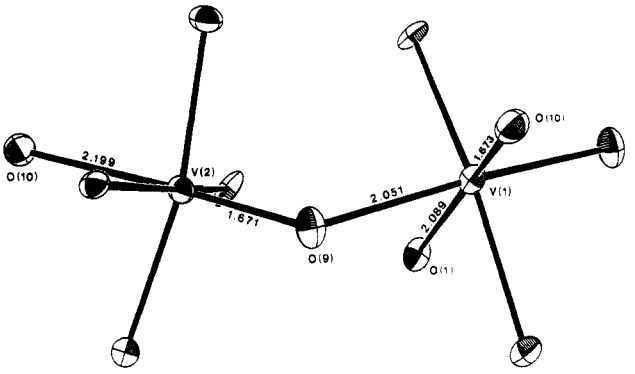


**Figure 2.** V coordination environment in KVP asymmetric unit.

in KTP. Table IV summarizes the octahedral distortions in KVP along with those of several other members of the KTP structural family for comparison.

The short V–O bond seen in KVP is typical of ionic compounds and extended structures containing the $VO^{2+}$ or "vanadyl" group. A simple model of the $VO^{2+}$ cation assumes a formal V–O double bond, which is observed as a very short V–O bond in some simple salts. For example, in vanadyl sulfate pentahydrate, $VOSO_4 \cdot 5H_2O$, one of the isolated V–O bonds is only 1.59 Å long.[17] However, in the continuous solid $VO_2$ (distorted rutile structure at room temperature) the distortion of the $VO_6$ octahedron is not nearly as exaggerated: the shortest V–O bond is 1.76 Å, while the average length of the other five V–O bonds is 1.97 Å.[18] Therefore, when compared to the bonding in $VO_2$, the short V–O bonds (1.671, 1.673 Å) found in KVP have strong formal double-bond character.[19]

Both phosphate groups have regular coordination distances, as in KTP ($d_{av}$ = 1.549 Å for both $PO_4$ tetrahedra), and the potassium atoms show no significant differences in coordination from those in KTP. K(1) in KVP is coordinated to eight oxygen atoms within 3.2 Å with an average K–O bond length of 2.854 (8) Å, while K(2) is 9-coordinate with an average bond distance of 2.925 (8) Å. In KTP, average K(1)–O and K(2)–O distances are 2.845 (4) and 2.934 (4) Å, respectively.

The indexed powder diffraction lines from KVP are presented in Table V. Lattice parameters of the KTVP composites are intermediate between those of KTP and KVP (Table VI) and follow Vegard's law.

### 3.2. Optical and Magnetic Properties

UV–visible spectra obtained on powder samples of KVP and the $KTi_{1-x}V_xOPO_4$ (KTVP) series at several values of $x$ are shown in Figure 3. The spectrum of pure KTP (spectrum a) shows an absorption inflection at 350 nm, with an onset at 370 nm. As expected, KTP remains transparent throughout the visible spectral

**Table V.** $KVOPO_4$ Powder Diffraction Data

| 2θ(Cu K) | $d$ spacing, Å | intens | $hkl$ |
|---|---|---|---|
| 13.837 | 6.3948 | 9 | 200 |
| 15.512 | 5.7076 | 20 | 110 |
| 16.222 | 5.4596 | 100 | 201 |
| 25.991 | 3.4255 | 20 | 212 |
| 26.519 | 3.3585 | 11 | 311 |
| 29.032 | 3.0732 | 94 | 203 |
| 30.120 | 2.9646 | 9 | 121 |
| 32.484 | 2.7540 | 49 | 221 |
| 32.837 | 2.7252 | 60 | 022 |
| 34.071 | 2.6293 | 17 | 004 |
| 35.791 | 2.5068 | 11 | 222 |
| 43.153 | 2.0946 | 7 | 130 |
| 44.635 | 2.0285 | 14 | 024 |
| 45.371 | 1.9973 | 6 | 205 |
| 50.170 | 1.8169 | 24 | 033 |
| 53.535 | 1.7104 | 17 | 424 |
| 54.186 | 1.6913 | 10 | 225 |
| 56.311 | 1.6324 | 6 | 216 |

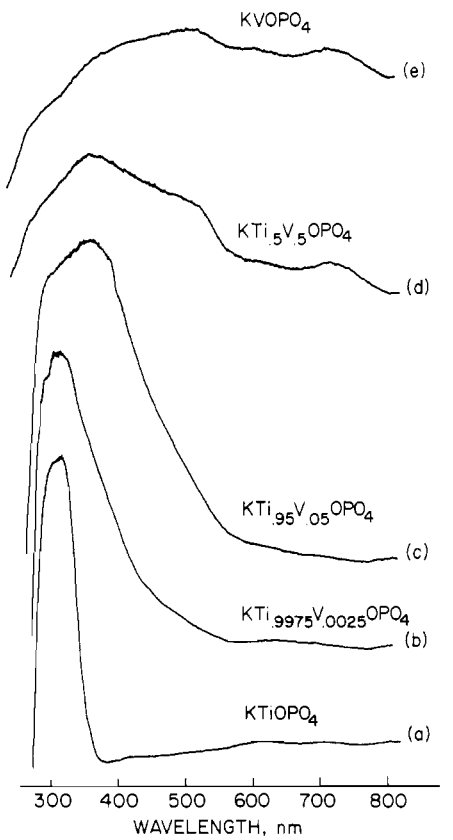


**Figure 3.** UV–visible spectra of $KTi_{1-x}V_xOPO_4$ at several values of $x$.

(17) Theobald, F.; Galy, J. *Acta Crsytallogr., Sect. B* **1973**, *B29*, 2732.
(18) Andersson, G. *Acta Chem. Scand.* **1956**, *10*, 623.
(19) In the undistorted $TiO_2$ (rutile) structure, the two Ti–O distances are 1.944 and 1.988 Å, and thus the distortion of the metal coordination sphere is increased in going from $TiO_2$ to $KTiOPO_4$ as well: Baur, W. H. *Acta Crystallogr.* **1956**, *9*, 515.

**Table VI.** Lattice Parameters and SHG Results for Several KTVP Compositions

| compd | *a*, Å | *b*, Å | *c*, Å | *V*, Å$^3$ | SHG intens (rel to KTP) |
|---|---|---|---|---|---|
| $KTiOPO_4$ | 12.831 (8) | 6.415 (2) | 10.578 (6) | 870.7 (8) | 1.0 |
| $KTi_{0.9975}V_{0.0025}OPO_4$ | 12.832 (9) | 6.414 (4) | 10.578 (6) | 870.6 (9) | 1.0 |
| $KTi_{0.95}V_{0.05}OPO_4$ | 12.812 (6) | 6.412 (7) | 10.582 (4) | 869.2 (10) | 0.13 |
| $KTi_{0.5}V_{0.5}OPO_4$ | 12.797 (5) | 6.397 (6) | 10.558 (6) | 864.2 (10) | 0.0008 |
| $KVOPO_4$ | 12.779 (9) | 6.373 (2) | 10.510 (2) | 855.9 (7) | N/A |

region. At low vanadium concentrations (spectrum b) there is no change in $\lambda_{max}$, though the absorption edge now has a long "tail" extending to 540 nm. As a result, samples of this material are a very pale yellow color. At the 5% V substitution level, $\lambda_{max}$ is shifted to 360 nm, leaving a shoulder at 320 nm. The tail on the absorption edge now extends deeply into the visible region, imparting a bright ochre color to the compound. In $KTi_{0.5}V_{0.5}OPO_4$ (spectrum d) the sharp peak gives way to a broad absorption ($\lambda_{max}$ = 360 nm), tapering off only slightly toward the red end of the spectrum, and in KVP (spectrum e) absorption is intense and nearly continuous throughout the wavelength range studied.

These spectra can be understood in terms of an interband electron transfer. In KTP, the absorption band in the UV region is due to a ligand-to-metal charge transfer between bonding orbitals localized on oxygen and antibonding orbitals localized on vanadium. As the vanadium concentration in KTVP is increased, the vanadium character of the excited state increases, since V(IV) is more oxidizing than Ti(IV).[20] The energy of the excited state is thus lowered, extending $E_g$ from the UV region through the visible region and into the IR region as $KVOPO_4$ is reached. Consequently, the excited-state MO cannot be localized on the $MO_6$ octahedra but must instead be delocalized along the O—M=O chain in a fashion analogous to conjugated $\pi$ systems in organic molecules and polymers.

It is expected from these spectral data that any 532-nm light generated by the combination of 1064-nm photons will be attenuated by absorption in the V-rich samples and should have weak second harmonic intensities. This is found to be the case, but it is not immediately predictable what effect doping by V(IV) in amounts not sufficient to cause excessive extinction of SHG light will have on SHG intensity. SHG data for the five compositions described above are reported in Table VI. These data do not demonstrate any influence in SHG intensity from the free electron other than what would be expected from absorption of second harmonic light, and in particular, the intensity from the 0.25% V-doped sample is not demonstrably different from KTP's. SHG intensity could not be reliably measured for KVP due to the generation of spurious light, although it is expected to have measurable SHG intensity at longer wavelengths. The lack of direct influence on optical nonlinearity by the extra electron on vanadium is predicted by theoretical considerations (section 3.3).

The average molar magnetic susceptibility of KVP at 5 K is 0.087 emu/mol, as expected for a paramagnetic transition-metal compound with a $d^1$ configuration. The magnetic susceptibility was measured between 5 and 50 K, and the reciprocal molar susceptibility varied linearly with temperature with no anomalies that might indicate a transition to an ordered (ferromagnetic or antiferromagnetic) state. KVP therefore remains paramagnetic at all measured temperature regimes, indicating that the superexchange overlap of vanadium p$\pi$ and oxygen p$\pi$ orbitals is negligible in this system.

### 3.3. Theoretical Discussion

The individual elements of the bulk susceptibility tensor of a NLO material, $\chi_{ijk}$, can be viewed as a vector sum of microscopic susceptibilities $\beta_{ijk}$ arising from individual bonds in the molecule or structure. Levine's bond charge theory describes these bond hyperpolarizabilities in terms of a bond charge residing in an anharmonic potential well.[21] The anharmonicity results from electronegativity and size differences between bonding atoms. A consequence of the harmonic oscillator model is the inverse dependence of the low-frequency linear susceptibility on the band gap, $E_g$. The magnitude of these microscopic hyperpolarizabilities depends strongly on the linear susceptibility in the medium due to the change of energy of the band gap orbitals and thus $E_g$.

In Levine's model, the microscopic susceptibility depends on bond length:

$$\beta = \beta_0(d/d_0)^\sigma \qquad (1)$$

where $\beta_0$ is the hyperpolarizability at the average bond length $d_0$, $\beta$ is the actual hyperpolarizability at bond length $d$, and $\sigma$ is a parameter calculated from observed bulk coefficients. The nonlinearity of the niobates and tantalates, in which the metal atom resides in a nearly octahedral field, is thus explained by the unequal contributions of the short and long bonds to the total susceptibility.

The limitations of this approach arise from the simplicity of the underlying assumptions of the model combined with the large number of parameters it must treat. Levine points out that the form of the dependence of $\beta$ on bond length in eq 1 is a fortuitous consequence of the bond charge model, which successfully predicts response for $LiNbO_3$ but predicts the second-order response of more complex niobates much less accurately. The model neglects cation–oxygen interactions, which have been shown to be significant in defining KTP's nonlinear response. The bond charge model also assumes negligible hyperpolarizability perpendicular to bond axes, that is, $\beta_\parallel \gg \beta_\perp$, an assumption that appears invalid in some systems.[22]

Using the bond charge model, Zumsteg et al. concluded that the difference in trans bond lengths is the primary contributor to KTP's second-order susceptibility.[1] This result was also obtained by Hansen et al. using electron density maps from single-crystal X-ray data to measure valence electron distribution in KTP.[23] Both studies assumed no significant contribution by K–O and P–O bond to $\chi_{ijk}$. Furthermore, Hansen's model predicts that the long Ti–O bonds make no significant contribution to the observed bulk susceptibility seen in KTP. However, the predicted response falls short of the experimentally determined $\Delta_{ijk}$ values.[24] Hansen et al. attribute this to the difficulty of predicting the variation of $\Delta$ with bond length.

The perspective of anharmonicity in NLO systems can be expanded from the earlier localized two-atom potential well model to a more delocalized anionic cluster, e.g. the $TiO_6^{8-}$ group in KTP. The hyperpolarizability of the electrons in this anionic group is viewed as a mixing of ground- and excited-state molecular orbitals. A group such as $TiO_6^{8-}$ whose excited-state dipole moment is very large would thus exhibit a large hyperpolarizability in the ground state provided the ground- and excited-state orbitals are close enough in energy to overlap. Several conclusions have been drawn from studies in which the anionic group model is applied to ionic and extended systems: (1) the cation (if any) plays little or no role in NLO behavior; (2) larger asymmetry of coordination in $MO_6$ octahedra results in larger microscopic hyperpolarizability; (3) when two oxygen octahedra share one oxygen atom, the NLO properties will depend entirely on $MO_6$ octahedra and their mode of distortion.[25] Good agreement with experimental $\Delta_{ijk}$ values

(20) Reduction potentials in aqueous solution at 298 K for the reaction $MO^{2+} + 2H^+ + e^- = M^{3+} + H_2O$ are +0.359 and +0.099 V for $VO^{2+}$ and $TiO^{2+}$, respectively: Huheey, J. E. *Inorganic Chemistry*, 3rd ed.; Harper & Row: New York 1983; pp A48–A49.

(21) Levine, B. F. *Phys. Rev. B* **1973**, 2600–2625.

(22) Bergman, J. G.; Crane, G. R. *J. Chem. Phys.* **1974**, *60*, 2470.

(23) Hansen, N. K.; Protas, J.; Marnier, G. *C. R. Acad. Sci. Paris, Ser. II* **1988**, *307*, 475–478.

(24) Normalizing the second harmonic tensor $\mathbf{d}_{ijk}$ with respect to the refractive indices of the medium yields $\Delta_{ijk}$ (Miller's $\Delta$), which is less sensitive to variations in linear susceptibility: Miller, R. C. *Appl. Phys. Lett.* **1964**, *5*, 17.

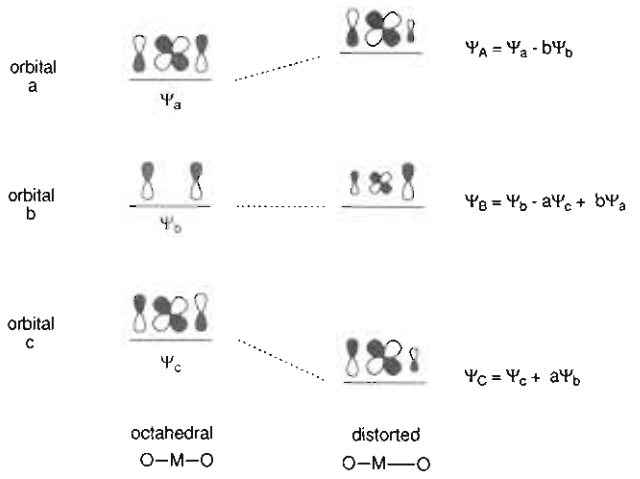


**Figure 4.** Mixing of ground- and excited-state M–O orbitals on distortion from octahedral symmetry.

is reported for a good number of simple metal oxide and nonmetal oxide crystals. The agreement between theory and experiment is not nearly as close, however, for highly distorted anion groups such as those found in KTP. In the discussion that follows, the arguments presented in the anionic group model that pertain to the KTP structure field are expanded to allow for electronic contributions to the framework orbitals from cations, tetrahedral groups ($PO_4$ and $AsO_4$) and electrons on the metal atoms themselves (e.g. KVP).

In our model, the distortion of the $MO_6$ octahedron is viewed in local terms by examining the orbitals of an octahedral $MO_6$ unit and observing how they mix as the geometry changes. Oxygen $p\pi$ and metal $d\pi$ orbitals mix to form bonding, nonbonding, and antibonding orbitals of g, u, and g symmetry, respectively. Simple perturbation theory allows access to the mixing of g and u orbitals during an asymmetric distortion (Figure 4). Both the interaction energies and the orbital mixing coefficients $a$ and $b$ depend upon the size of the energy gaps and the overlap integrals between the relevant orbitals at the octahedral geometry. The magnitudes of the mixing coefficients both at the octahedral geometry and on distortion are readily obtained via a simple extended Hückel calculation. There is clearly an electronic stabilization associated with the distortion, and it is the competition between this effect and the destabilization associated with other occupied orbitals that controls the actual magnitude of the distortion on the one-electron model. Significantly, the orbitals of Figure 4 are intimately connected with the nonlinear optical properties of the system.

Using the expression for the nonresonant second-order hyperpolarizability (eq 2) evaluated via perturbation theory gives some insight into the changes expected as a function of local structure:

$$\beta_{rst} = \pi^2 \sum_{P} \sum_{e,e'} \langle g|\mu_r|e\rangle\langle e|\mu_s|e'\rangle\langle e'|\mu_t|g\rangle / h\omega_e h\omega_{e'} \qquad (2)$$

where

$$\omega_e = \omega_e - \omega_g - 2\omega \qquad \omega_{e'} = \omega_{e'} - \omega_g - \omega$$

Here, $|g\rangle$ is the electronic ground state and $|e\rangle$ and $|e'\rangle$ are excited states. $\omega$ is the frequency of the incident radiation. The first sum in eq 2 is over the various combinations of the dipole moment operators $\mu_t$. Given the geometry, we can compute the contribution to $\beta$ or more precisely, how the contribution varies with distortion, though we cannot calculate the lowest energy conformation for a given system.

A complete calculation would contain the excitations appropriate for a band structure computation on the material, but here we will use results from an octahedrally coordinated metal atom. Accordingly, our results will become more meaningful as the

(25) Chen, C.-T. *Annu Rev. Mater. Sci.* **1986**, *16*, 203–243 and included references.

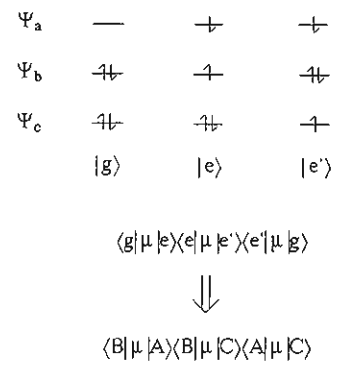


**Figure 5.** Orbital occupancy of ground and excited states in $TiO_6^{-8}$ unit.

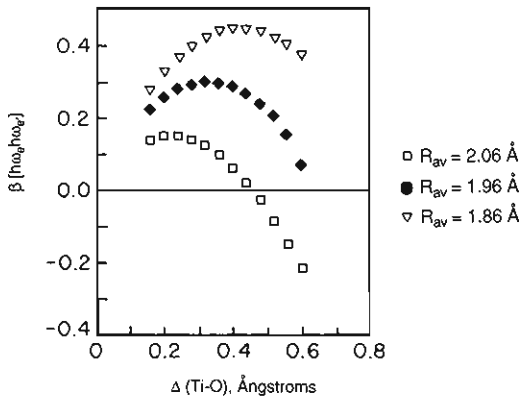


**Figure 6.** Dependence of nonlinear polarizability on average M–O bond distance ($R_{av}$) and on short–long metal–oxygen bond length difference ($\Delta$).

asymmetric distortion increases and the orbitals become more localized. We can readily calculate the matrix elements appearing in the numerator of eq 2 for such a model. Notice that the three-center problem is associated with the $\pi$ levels of the unit. The metal atoms of most materials under consideration (except KVP) are in a $d^0$ configuration, so that orbitals of $\pi$ symmetry comprise the highest occupied orbital of the molecule and highest occupied band of the solid. There are thus the most important in the perturbation expression of eq 2. Of the three lowest unoccupied energy levels of the unit, one is of $\delta$ symmetry with respect to the O–M–O chain, and it will be ignored for the present. This orbital becomes important when the effects of the extra d electron in KVP are contemplated. Figure 5 shows the orbital occupancy of the three states $|g\rangle$, $|e\rangle$, and $|e'\rangle$. We will just consider the orbitals associated with one $\pi$ component. (Our results for the axially symmetric case will just need to be multiplied by 2.) Each may be written as an antisymmetrized serial product of the relevant occupied molecular orbitals, and it easy to see that the triple product of the numerator of eq 2 involving wave functions describing electronic states reduces to one which contains molecular orbital functions only (eq 3).

$$\langle B|\mu|A\rangle\langle B|\mu|C\rangle\langle A|\mu|C\rangle \qquad (3)$$

We now observe how this triple product varies with the magnitude of the asymmetric distortion. First we note that at the undistorted geometry with a center of symmetry the last term in this expression is identically zero since it couples two symmetric levels via an antisymmetric operator. The dipole moment operator in this equation will only have nonzero components along the O–M–O axis on our model. The results thus obtained will therefore be relative to a local axis frame and to be compared with experiment should take into account the relationship of these local axes to the crystal axes.

Our calculations show that the change in the compared energies of the orbitals concerned on distortion is rather small but that there are considerable changes in the nature of the orbitals concerned. Thus, it is the value of the numerator that contains the important information for our needs. Figure 6 shows the computed results

for the variation in the numerator of eq 2 as the distortion progresses from an undistorted structure with a given Ti–O distance ($R_{av}$). $\Delta$ is the difference in the two trans Ti–O distances and $R_{av}$ is the average of the two equilibrium Ti–O distances. Notice that the plot indicates that there is a maximum in the hyperpolarizability along with a change in sign for large distortions. This is a result that parallels that of Levine, obtained via a very different model.

The maximum in the value of the numerator appears at larger $\Delta$ with a smaller $R_{av}$, yielding a larger value of $\beta$. That there is a maximum in the plot is easy to understand. Of the three terms appearing in the numerator, two ($\langle b|\mu|a\rangle$ and $\langle b|\mu|c\rangle$) are nonzero at the symmetrical geometry with $\Delta = 0$, but the third, $\langle a|\mu|c\rangle$, is zero. On distortion the first two decrease in magnitude, but the third increases from zero. For $R_{av} = 1.94$ Å, which is close to $R_{av}$ values found experimentally for the bonds around Ti(1) in $KTiOPO_4$, $NH_4TiOPO_4$ and $KTiOAsO_4$, the maximum is calculated to occur at around $\Delta = 0.32$ Å, somewhat smaller than the values actually found in these systems. (The bonds around Ti(2) are slightly shorter on average, with typical $R_{av}$ values of 1.92 Å.) See Table IV.

We can now use this model to predict the electronic effects of varying the chemical composition in the KTP structure field, beginning by replacing $Ti^{IV}$ with $V^{IV}$ to yield $KVOPO_4$. KVP is thus a $d^1$ species and contains at 1.673 Å the shortest M–O distance found in any KTP isostructure. This very short distance ensures that the two $\pi$ orbitals involved in this linkage are pushed to high energy and that the lone electron lies in an orbital of $\delta$ symmetry with respect to the O–V–O axis. As explained in section 3.2, the effect of this extra electron on the nonlinear properties of KVP cannot be determined by SHG experiments using near-IR pump beams due to the opacity of this material to visible and near-IR radiation. However, it is expected that the influence of the extra electron may be neglected, in the first order at least, since these $\pi$ and $\delta$ orbitals are orthogonal. The SHG intensity measurements on the KTVP compounds using 1.064-$\mu$m light (section 3.2) tend to support this assertion, as low concentrations of vanadium do not appear to influence SHG intensity.

We can also understand some of the variations in NLO properties found among $MTiOPO_4$ compounds. It has been found experimentally that the SHG intensities of $AgTiOPO_4$ (AgTP) and $\beta$-$NaTiOPO_4$ (NaTP) are substantially less (1/1000 and 1/10 for AgTP and NaTP, respectively) than that of KTP. Since the $R_{av}$ and $\Delta$ values (Table IV) for these compounds are close to those of KTP, it is obvious that bond-length asymmetry arguments alone cannot tell the whole story. This model leads to some further insight into the cation dependence of $\beta$ in terms of the variation of the orbital mixing coefficients of the framework orbitals with the ionicity of the cation–framework interaction. Because the magnitude of the numerator of eq 2 depends on the size of the coefficients of orbitals located on the $MO_6$ framework, a process that causes a decrease in their contribution to the wave functions concerned should lead to a decrease in the value of the numerator for a given value of $\Delta$ and $R_{av}$. As the structure becomes less ionic, the occupied orbitals become less frameworklike. Thus, decreasing the ionicity by reducing the coordination number of the cation and/or by increasing its electronegativity should in general lead to this result. Ag is more electronegative than K and has a smaller coordination number in AgTP (CN = 5 and 4 in Ag(1) and Ag(2), respectively) than does K in KTP (CN = 8 and 9 in K(1) and K(2)), resulting in lower cation–framework ionicity. We thus predict that the nonlinear optical response of $AgTiOPO_4$ should be much lower than that of KTP, and this is exactly what is observed, even though the Ti–O bond asymmetry in AgTP is nearly identical with KTP's.

The cation coordination numbers of NaTP, at 7 and 5 for Na(1) and Na(2), are nearly the same as those for AgTP, and the SHG intensity of NaTP is much less than that of KTP.[9,10] This effect is moderated by the more electropositive nature of the $Na^+$ ion, and the loss of SHG intensity is less here than in AgTP. In $TlTiOPO_4$ however, the NLO properties are similar to those of the potassium analogue, despite the electronegativity difference between K and Tl. We are currently investigating the structural and optical properties of TlTP, including the stereochemical role of the 6s lone pair electron on $Tl^+$ and will report the results in the near future.[26]

A related result is associated with the replacement of As for P in the $TO_4$ unit. Phosphorus is more electronegative than arsenic, and we expect a larger admixture of phosphorus orbitals into the framework oxygen levels than for arsenic, a result supported by calculation. This may provide an explanation for the experimental observation of improved nonlinear optic and electrooptic properties of KTA relative to KTP.

This model is a simple one and should be applied cautiously. We have assumed axial symmetry for the O–M–O unit, whereas in the solids concerned the angle at the oxygen atom joining the two $M_1$ and $M_2$ atoms is somewhat less than 180°. Also there is probably a range of distances for which the scheme is valid. For $\Delta = 0$ we should use a band description of the solid, and for very large distortions the middle orbital on our scheme is completely oxygen localized. We have performed band structure calculations for these materials, and for the values of $\Delta$ typically found in practice, the sizes of the orbital coefficients and their general behavior as the system is made asymmetric certainly follow the trends we have discussed. The model is thus valid for the degrees of distortion found in the KTP isostructures and should be realistic for metal oxides with asymmetric distortions of the same order.

## 4. Summary

In this paper we have reported the structure and optical properties of $KVOPO_4$, a compound isostructural with the important NLO material $KTiOPO_4$ (KTP). Vanadium(IV) substitution resulted in the shortest octahedral M–O bond distance reported in the KTP structure field to date. With V substitution for Ti in the KTVP series the band edge broadens and shifts to longer wavelengths as the excited state, which is delocalized along the O—M═O chain, acquires more V character. Increasing vanadium concentration does not appear to alter SHG other than by attenuating the emergent second harmonic beam. KVP remains paramagnetic at liquid-helium temperatures, indicating that magnetic ordering, which would take place via overlap of metal $d\pi$ and oxygen $p\pi$ orbitals, does not occur to a measurable extent.

We have extended the anionic group model of second-order susceptibility, modeling electronic influences from nonbonding ($t_{2g}$) electrons, cations, and tetrahedral framework atoms. Three conclusions are noted: (1) $t_{2g}$ electrons on framework metal atoms have no effect on optical nonlinearity; (2) higher ionicity of the cation–framework interaction results in increased NLO response; (3) decreasing the electronegativity of the tetrahedral atom (e.g. substituting As for P) also results in increased NLO response. Experiments that will allow us to better define structural and electronic contributions to NLO susceptibility and design new materials with improved nonlinear optical properties are continuing.

**Acknowledgment**. This work was supported by the National Science Foundation Division of Materials Research (G.D.S. and J.K.B.) and by Du Pont (G.D.S.). We thank Dr. Nancy Keder for her help in obtaining crystallographic data on KVP and Dr. Bob Dunn for his assistance in collecting the magnetic susceptibility data. Conversation with Dr. Peter C. Ford concerning the spectral data has also proved valuable.

**Supplementary Material Available:** Tables of anisotropic thermal parameters and all bond distances and angles within 3.4 Å (2 pages); a table of calculated and observed structure factors (5 pages). Ordering information is given on any current masthead page.

(26) Harrison, W. T. A.; Gier, T. E.; Stucky, G. D.; Schultz, A. J. *J. Chem. Soc., Chem. Commun.*, in press.
(27) Keder, N. L.; Gier, T. E.; Stucky, G. D. Unpublished results.
(28) El Brahimi, M.; Durand, J. *Rev. Chim. Mineral* **1986**, *23*, 146.
(29) Phillips, M. L. F.; Harrison, W. T. A.; Stucky, G. D. Unpublished results.
(30) Phillips, M. L. F.; Harrison, W. T. A.; Stucky, G. D. *Inorg. Chem.*, in press.